Science and Technology Indonesia
e-ISSN:2580-4391 *p*-ISSN:2580-4405
Vol. 11, No. 2, April 2026

Research Paper

The Influence of Milling on the Structural and Morphological Properties of Waste-Based Active Carbon from Rubber Seeds Using High Energy Milling (HEM) Method

Fitri Suryani Arsyad[1,2*], Aprilianda[1], Aulia[1], Akmal Johan[1], Ihsan Alfikro[1], Amiruddin Supu[3], Nur Ahmad[4], Andrivo Rusydi[5]

[1]*Department of Physics, Faculty of Mathematics and Natural Sciences, Universitas Sriwijaya, Ogan Ilir, South Sumatera, 30662, Indonesia*
[2]*Master Program of Materials Science, Graduate School, Universitas Sriwijaya, Palembang, 30139, Indonesia*
[3]*Department of Physics Education, Faculty of Teacher Training and Education, Universitas Nusa Cendana, East Nusa Tenggara, 85001, Indonesia*
[4]*Research Center for Catalysis, National Research and Innovation Agency (BRIN), Serpong, South Tangerang, 15314, Indonesia*
[5]*National University of Singapore, Queenstown, 119077, Singapore*
***Corresponding author**: fitri_suryani@unsri.ac.id

Abstract
The high-energy milling (HEM) synthesis method has produced activated carbon powder from rubber ore shell waste. The activated carbon was prepared using a chemical method with activation temperatures varying between 400, 500, and 600°C. Temperature optimization resulted in activated carbon with a maximum carbon content at 600°C. The activated carbon was then milled for various times: 0, 30, 60, and 90 minutes. The crystallinity and surface morphology of the samples were then confirmed using an X-ray diffractometer (XRD) and scanning electron microscope (SEM) characterization. Based on the XRD graph, the percentage of structural regularity, or degree of crystallinity, of the activated carbon tended to decrease from 18.17% without milling treatment to 17.52% at 30 minutes of milling, 17.45% at 60 minutes of milling, and 17.35% at 90 minutes of milling. SEM images also show a decrease in the average pore diameter from approximately 0.45 µm to 0.20 µm with a more homogeneous intraparticle morphology structure when the milling time is increased from 30 minutes to 90 minutes. This study demonstrates the potential of rubber seed shell waste for processing into activated carbon. The HEM method can significantly reduce the grain size of activated carbon and increase its surface area and reactivity, making it more effective in applications as an adsorbent and filter.

Keywords
Rubber Seed Shell, Activated Carbon, HEM, Milling Time, Temperature

Received: 9 May 2025, Accepted: 30 January 2026
https://doi.org/10.26554/sti.2026.11.2.621-631

1. INTRODUCTION

Indonesia is one of the biggest rubber-producing countries in the world. Rubber producers in Indonesia are widespread in various provinces, including South Sumatra, with a total rubber land area of around 872,503 hectares (Center for Agricultural Data and Information Systems, 2020). Most natural rubber is used as a raw material for making tires (Phiri et al., 2021) seals and various forms of padding for several motor vehicle parts (Prasad et al., 2020) to make floors as an adhesive or protective layer for many surfaces (Li et al., 2020).

Rubber seeds are considered to have lower economic value, thus becoming unused waste. In fact, with proper processing, rubber seed waste can be used as raw material for biodiesel (Tarigan et al., 2022; Sambasivam et al., 2023), as a biocatalyst (Oladipo and Betiku, 2020), as a food source (Udo et al., 2018), and as activated carbon (Nguyen et al., 2023; Fatima et al., 2023). Organic rubber shells contain several chemical components, such as cellulose, hemicellulose, and lignin, which are suitable for carbon production (Zeng et al., 2024).

Activated carbon is a material made from amorphous carbon compounds obtained from natural materials containing carbon (Sasmita et al., 2022) and charcoal from combustion or other treatments, resulting in a larger and more uniform surface area, according to Fatima et al. (2023). To evaluate the quality of activated carbon produced from biomass, a commonly used analysis is proximate analysis. This analysis is used by determining the content of water, ash, volatile matter, and fixed carbon, which are critical indicators for the adsorption performance and purity of the material (Hamid et al., 2024; Divya et al., 2025). Figure 1 shows the hexagonal carbon atom arrangement of activated carbon, which is covalently bonded at each corner (McEnaney, 1999).

In general, activated carbon is often used as an adsorbent to purify water (Devi et al., 2023) and as Norit (diarrhoea medicine) in the medical world (Heimesaat et al., 2024; Torvorapanit et al., 2023). It is used as a water filter in the water

filtration industry (Roy et al., 2023; Zuo et al., 2019), air filter (Mohan et al., 2019), and beauty industry (?).

Activated carbon is made through three stages. The first is a dehydration process where the raw material is heated at a specific temperature until there is no more water in the carbon raw material, then carbonized (charcoal), and the last is activated chemically or physically (Patel et al., 2024; Tonu et al., 2024). Yossaa et al. (2020) made activated carbon from Biobab seed coats using a chemical activation method and successfully compared the rate of diuron absorption kinetics in mesopore and micropore-activated carbon. Gao et al. (2024) also wrote an extensive literature review on the insight of chemicals as carbon activation process agents. According to Zhu et al. (2022), the chemical activation method has various advantages over physical activation methods, among others: chemical activation is available in the preparation process, so that the carbonization steps and the carbonization process are summarized in one step, which is generally called one-step activation. The product produced by the chemical activation process is much more than the physical activation process (Nurfarhana et al., 2023). Therefore, in this study, activated carbon was synthesized using chemical activation.

Our previous research successfully processed rubber seed shell waste into activated carbon using a carbonization process at 600°C (Aulia et al., 2019). Based on a literature review, no research has been found that explicitly combines high-energy milling (HEM) with rubber seed shells after activation. Therefore, in this study, to investigate the HEM aspect, the activated carbon produced was subsequently ground using HEM. The aim was to enhance its structural, morphological, and particle size properties. In this study, rubber seed shell activated carbon was ground for less than 1 hour, specifically 30, 60, and 90 minutes. The next step was material characterization analysis to study the effect of grinding time on structural properties and surface morphology using XRD and SEM.

2. EXPERIMENTAL SECTION

2.1 Reagents

Rubber seed shell waste was used as the carbon precursor in this study. The raw material was collected locally, washed with tap water to remove surface impurities, and dried before carbonization. Phosphoric acid (H_3PO_4) aqueous solution with a concentration of 7% (v/v), analytical reagent (AR) grade, purchased from Chemical Express, was used as a chemical activating agent during the activation process. Distilled water (aquades) was used for washing and neutralizing the activated carbon samples until a neutral pH was achieved after chemical activation. Deionized water was used as a medium for density and porosity measurements. All chemicals were used as received without further purification.

2.2 Initial Processing of Rubber Seed Shells into Charcoal

The process of making activated carbon goes through 3 stages. The first stage is the dehydration process, where the rubber seed shells are dried in the sun for 12 hours to remove the water content in the shells. Next, the carbonization or charring process is carried out, namely, the rubber seed skin is burned for 30 minutes at different temperatures, 400, 500, and 600 °C, until it becomes charcoal. The charcoal formed is then pulverized and sieved with a size of 100 mesh (Aulia et al., 2019).

2.3 Carbon Activation Process

After the carbonization process, rubber seed coat charcoal is chemically activated into activated carbon by soaking in an H_3PO_4 solution for 24 hours. The goal is to open, enlarge, or expand the pore dimensions. The resulting activated carbon is then filtered and rinsed using distilled water until the pH is neutral. Furthermore, it is dried in the oven at 105 °C. The quality of activated carbon was analyzed by calculating ash content, moisture content, volatile substance content, fixed carbon content, and finally, its functional groups using Fourier Transform Infra-Red (FTIR) analysis (Aulia et al., 2019).

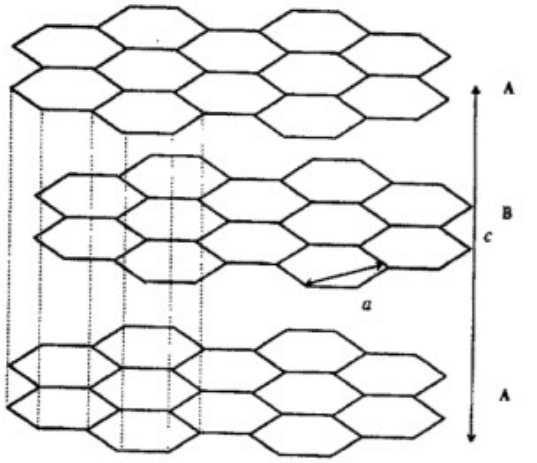

Figure 1. The Hexagonal Lattice Structure of Activated Charcoal Graphite (McEnaney, 1999)

2.4 Activated Carbon Milling Process

To reduce the particle grain size, the activated carbon that has been made is then milled using high-energy milling (HEM). Before milling, the activated carbon that has been made is then weighed using an analytical balance and milled using HEM with a sample weight ratio and ball milling of 1:5. The milling process was carried out with the on-off method for 10 minutes for 30 minutes, 60 minutes, and 90 minutes, respectively. To determine the nature of the structure and surface morphology, the milled activated carbon was then characterized using XRD and SEM (Milyutin et al., 2023).

2.5 Material Characterization

Infrared (IR) spectroscopy was used to analyze the functional group in the 4000 to 400 cm^{-1} frequency range using an IR Prestige21 Shimadzu. The morphology images of particles

Table 1. Results of the Carbon Bath on the Effect of Carbonization Temperature

Data on Charcoal Produced	Temperature of Carbonization		
	400 °C	500 °C	600 °C
Mass of rubber seed shell (g)	55	55	55
Charcoal mass (g)	20.936	17.758	15.233
The mass lost (g)	34.064	37.242	39.767
% Charcoal yield	38.065	32.287	27.696
% The mass lost	61.934	67.712	72.303

were obtained by scanning electron microscopy (SEM) model TESCAN VEGA II. Particle size distribution of carbon particles was calculated by ImageJ software with a Java preinstalled to measure distances determined by the area and pixel statistics. The X-ray diffraction was carried out on the Rigaku Miniflex 600 model.

3. RESULT AND DISCUSSIONS

3.1 Analysis of the Effect of Carbonization Temperature on the Quality of Charcoal

The carbonisation process consists of four stages: evaporation of water, evaporation of cellulose, evaporation of lignin, and purification of carbon. It is known that the lignin evaporation process requires temperatures above 300 °C, while the carbon purification process requires temperatures around 500 °C to 600 °C. This is done to obtain a good-quality charcoal yield (Swiątkowski et al., 2024; Togibasa et al., 2021). After the carbonization process is complete, the charcoal yield calculation process is carried out using Equation (1) (Hamid et al., 2024; Divya et al., 2025),

$$\text{Yield} = \frac{m_a}{m_b} \times 100\% \tag{1}$$

where m_a is the mass of the rubber seed shell after burning (g) and m_b is the mass of the rubber seed shell (g). The aim is to determine the difference between the mass of the rubber seed shell and the charcoal produced, and to see the effect of increasing carbonization temperature on the quality of the charcoal. The use of higher temperatures in the carbonization process results in a decrease in the obtained yield. This is because increasing the carbonization temperature increases the reaction between carbon and water. More carbon reacts to become CO_2 and H_2, resulting in a smaller amount of carbon (McEnaney, 1999). Table 1 shows the yield data of charcoal produced by those changes due to an increase in carbonization temperature. An increase in the rubber skin carbonization process's temperature from 400 °C to 600 °C will decrease the percentage of soaking produced from 38.065% to 27.696%. The increasing carbonization temperature causes the reaction between C and H_2O to increase, decreasing the charcoal bath. C binds more to CO_2 and H_2.

3.2 The Quality Test Analysis of the Activated Carbon

After the yield data were obtained, rubber seed shell charcoal was activated using H_3PO_4 with a ratio of 1:4. After the carbon activation process, quality test analysis was carried out by calculating the moisture content, ash content, volatile substances, and fixed carbon. Several international studies have used proximate analysis to assess the quality of activated carbon, including parameters such as moisture content, ash content, volatile matter, and fixed carbon. Divya et al. (2025) produced activated carbon from bamboo using H_3PO_4 activation and reported moisture, ash, volatile, and fixed carbon values as indicators of activated carbon product quality in accordance with ASTM standards. This proximate analysis uses Equations (2)-(4), as conducted by Hamid et al. (2024) and Divya et al. (2025):

$$\text{Moisture Content (MC)} = \frac{m_a - m_b}{m_{sample}} \times 100\% \tag{2}$$

m_a is the mass of the sample + cup before the oven (g), m_b is the mass of the sample + cup after the oven (g), and m_{sample} is the mass of the activated carbon sample before the water content test (g).

$$\text{Ash Content (AC)} = \frac{m_{ash}}{m_{sample}} \times 100\% \tag{3}$$

m_{ash} is the mass of the sample after becoming ash (g), and m_{sample} is the initial mass of the activated carbon sample before ash (g).

$$\text{Volatile Matter (VM)} = \frac{m_a - m_b}{m_{sample}} \times 100\% \tag{4}$$

m_a is the mass of the sample before being tested for volatile matter content (g), and m_b is the mass of the sample after being tested for volatile matter content (g).

$$\text{Fixed Carbon (FC)} = 100\% - (MC + AC + VM) \tag{5}$$

MC (Moisture Content) is the moisture content (%), AC (Ash Content) is the ash content (%), and VM (Volatile Matter) is the volatile matter content (%). From Table 2, in addition to affecting the percentage yield of carbon charcoal, the carbonization temperature also affects the quality value of the activated carbon that has been produced. Activated carbon at a temperature variation of 600 °C during the carbonization process produced quality values that tended to be closer to the quality standard values or predetermined standards than activated carbon produced by carbonization with temperature variations of 400 °C and 500 °C.

Table 2 shows the change in the quality of activated carbon due to an increase in carbonization temperature. From the results of the calculation of the moisture content of the rubber seed shell activated carbon (Equation 2), the water content at

Table 2. The Quality of Activated Carbon is Due to the Carbonization Temperature

Type of Test	Standards	400°C (%)	500°C (%)	600°C (%)
Moisture Content	Max. 15%	3.21	2.67	2.03
Ash Content	Max. 10%	0.99	2.09	2.57
Volatile Matter	Max. 25%	32.89	26.70	19.64
Fixed Carbon	Min. 65%	62.51	69.14	76.15

400 °C decreased from 3.21% to 2.03% due to the increase in temperature to 600 °C. The decrease in the percentage of water content due to the high-temperature ashing process has also been previously confirmed in Swiątkowski et al. (2024) and Neme et al. (2022) research. This is because the higher the temperature, the more the dehydration process in carbon increases, so the water content decreases. Low water content can increase activated carbon absorption.

Table 3. The Effect of Carbonization Temperature on the Value of the Density and Porosity of Activated Carbon

Temperature Variations (°C)	Density (g/cm^3)	Porosity (%)
400	0.01198	7.689
500	0.01193	13.202
600	0.01182	14.809

Another quality standard is ash content. The standard ash content for powdered activated carbon is 10%. The ash content dramatically affects the quality of the charcoal produced. Excessive ash content can clog the pores of the charcoal, so that the surface area is reduced (Swiątkowski et al., 2024; Neme et al., 2022). Based on the calculation of ash content using Equation (3), it is obtained that the increase in temperature in the carbonization process from 400 °C to 600 °C affects the higher ash content, which is 0.99% to 2.57%. The increase in ash content is due to mineral salts forming during the carbonization process. These mineral salts are derived from the starting material for carbon-producing biomass. When carbonization is continued, these mineral salts will form fine particles. These mineral materials will form new compounds, namely ash, when treated through an oxidation process.

Next is the volatile matter test. This volatile matter test is a standard test of activated carbon quality to determine and analyze the levels of volatile substances in activated carbon produced at a temperature of 950 °C. The volatile matter test for powdered activated carbon is 25%. The volatility level is influenced by charcoal's chemical components, such as the presence of extractive substances from rubber seed shell charcoal (Swiątkowski et al., 2024; Neme et al., 2022). From the calculation results using Equation (4), obtained the increasing carbonization temperature from 400 °C to 600 °C decreased the volatile matter content, initially from 32.89% to 19.64%. The amount of volatile matter is determined by two factors, namely the effect of the length of time and the temperature of carbonization. Increasing the carbonization temperature will affect the amount of substance wasted due to high evaporation, resulting in a lower substance content.

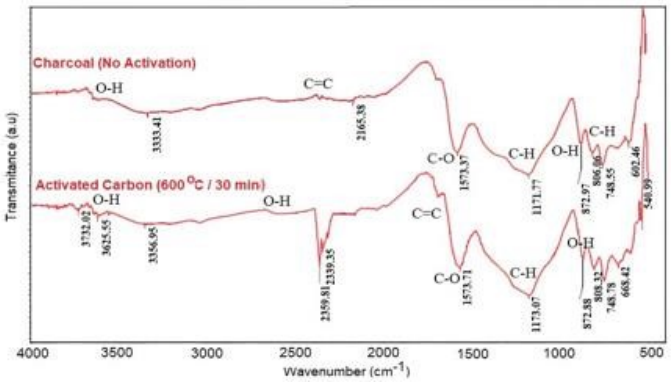

Figure 2. FTIR Spectrum of Carbon Without the Activation Process and With the Activation of the Rubber Seed Shell Raw Material

The substance that evaporates is the substance that will cover the surface of the cavities formed in the carbon. The more that evaporates, the more carbon pores are opened, and the greater the activated carbon absorption. Finally, the fixed carbon test is calculated using Equation (5). This test aims to determine the content of the bound carbon in the sample. The fixed carbon test for powdered activated carbon is at least 65%. Table 2 shows the effect of increasing the carbonization temperature from the initial temperature of 400 °C to 600 °C on the quality of the volatile matter content, which also increases from 62.51%–76.15%. One factor that affects the value of the bound carbon content of activated carbon is the initial carbon content contained in the initial raw materials used. The activation method and temperature are other factors that affect pure activated carbon and charcoal. In addition, the natural content of raw materials such as cellulose and lignin also affects the carbon yield. The results of this study show that lower water and ash content, accompanied by higher fixed carbon content indicates successful chemical activation, in line with the trend reported in activated carbon studies published in Science and Technology Indonesia (Wardani et al., 2021). A density and porosity test is performed to determine the density of the substance or particle and the pore size of the activated carbon that has been made. The density (Equation 6) and porosity (Equation 7) of activated carbon were calculated using the Equations

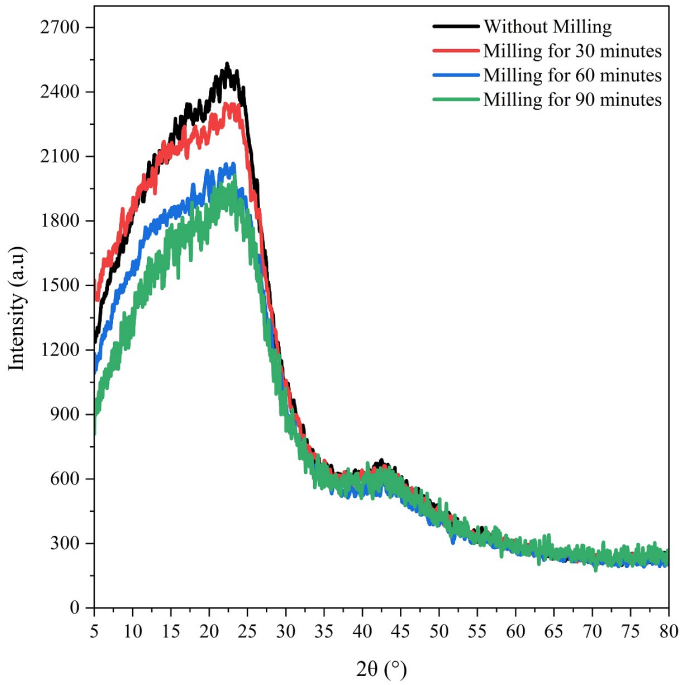

Figure 3. Diffraction Pattern of Activated Carbon Based on the Variation of Rubber Seed Shell Milling Time

as follows Divya et al. (2025):

$$\rho = \frac{m_3 - m_1}{(m_2 - m_1) - (m_4 - m_3)} \quad (6)$$

where, m_1 = mass of pycnometer (g), m_2 = mass of pycnometer containing water (g), m_3 = mass of pycnometer containing powder (g), and m_4 = mass of pycnometer containing powder and water (g),

$$\text{Porosity (\%)} = \frac{V_{solution} + V_{material} - V_{combined}}{V_{material}} \times 100\% \quad (7)$$

where, $V_{solution}$ = volume of water (cm^3), $V_{material}$ = volume of powder or sample (cm^3), and $V_{combined}$ = volume of water+powder (cm^3).

Table 3 shows that the Density of the activated carbon did not change significantly, from 0.01198 g/cm^3 to 0.01182 g/cm^3. Although the carbonization temperature increased from 400 °C to 600 °C, its porosity rose from 7.689% on carbon. This is because, in the combustion process, the particle arrangement of material will be more regular, so that the charcoal pores open more with increasing carbonization temperature (Swiątkowski et al., 2024; Marcilla et al., 2000).

3.3 Analysis of Functional Groups of Rubber Seed Shell-Activated Carbon using FTIR Characterization

FTIR characterization is used to identify a compound's functional groups through the compound's infrared absorbance band. The transmittance and absorption patterns of different absorbed compounds have their characteristics, making it possible to analyze the differences and quantify these compounds. FTIR test is only carried out on activated carbon carbonized at 600 °C because it has better quality than activated carbon carbonized at 400 °C and 500 °C.

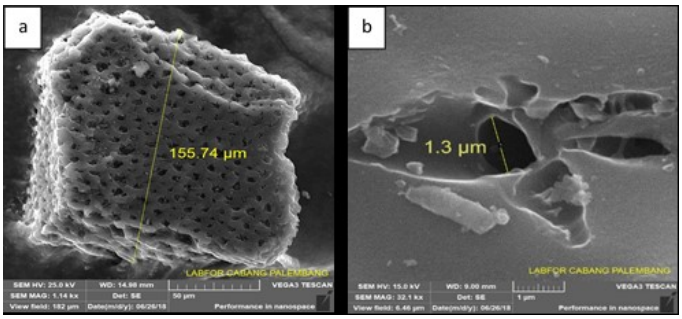

Figure 4. SEM Image of Activated Carbon Before Milling with SEM Image Magnification of 1.14 kx (a) and 30 kx (b)

Figure 2 shows the percentage spectrum of the transmittance of the formation of functional groups from carbon (a) without an activation process (b) activated carbon from FTIR characterization. Figure 2 above shows the formation of functional groups by adjusting some compounds from Carbon material without an activation process, and with activation has the same functional groups are formed at wave numbers 1573 cm^{-1}; 1173 cm^{-1}; 872 cm^{-1}; 808 cm^{-1}; and 748 cm^{-1}, which a functional groups C=C; CO; CH, and OH. However, there is a decrease in the transmittance value of activated carbon at a wave number of 2359.8 cm^{-1}. The H_3PO_4 activator causes the OH vibration in the P-OH group (Sarif et al., 2023; Yang et al., 2020). In addition, the activated carbon from the synthesis of this work also confirmed the presence of P-OH, O-H, and C-H aliphatic functional groups.

3.4 Analysis of the Effect of Milling on Structural Properties and Morphology of Activated Carbon

The milling process is a refining process that is carried out to produce nano-sized particles of activated carbon. One of the tools that can be used to make nano-sized particles is High Energy Milling (HEM). In this work, the activated carbon of the rubber seed shell was milled with time variations for 30, 60, and 90 minutes. Then the structural properties were characterized using XRD.

The aim is to see the diffraction pattern of the activated carbon crystals and the degree of crystallinity. The diffraction pattern of rubber kernel shell-activated carbon can be compared with the diffraction pattern of graphite carbon. X-ray investigations show that activated carbon is a tiny crystal similar to the structure of graphite (Keppetipola et al., 2021). The results of the activated carbon synthesis have a close-packed hexagonal (HCP) crystal structure, which is valid for graphite. However, activated carbon has a higher degree of regularity in the crystal structure. Activated carbon has an amorphous

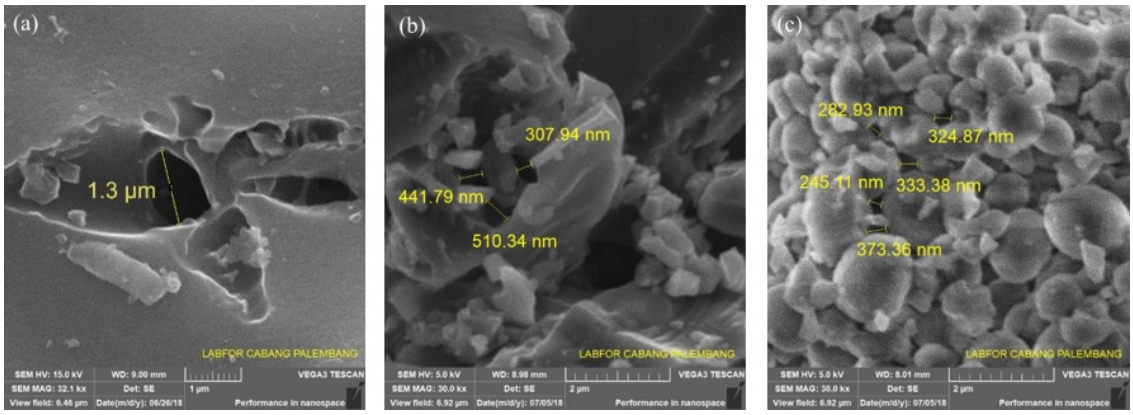

Figure 5. Photograph of SEM of Activated Carbon of Rubber Seed Shell (a) Before Milling, (b) Milling for 30 Minutes, and (c) Milling For 90 Minutes, with SEM Image Magnification of 30 k×

structure that is expected to have a diffraction pattern close to the graphite diffraction pattern, so that graphite can become a standard reference for activated carbon.

Table 4. Structural Properties of Activated Carbon of Rubber Seed Shell Based on Milling Time Variation

Milling time (minutes)	θ_B (°)	Intensity (cps)	Degree of crystallization (%)
0	12.58	2158.6	18.17
30	12.56	2068.4	17.52
60	12.57	1839.8	17.45
90	12.56	1800.2	17.35

Figure 3 is the result of X-ray diffraction patterns for activated carbon in rubber seed shells with milling treatment of 0 minutes (A), milling 30 minutes (B), milling 60 minutes (C), and milling 90 minutes (D). From this figure, there is a decrease in the intensity of the diffraction peak when the activated carbon powder is milled with variations in the milling time. The peak intensity of non-milled activated carbon was approximately 2158.6 cps (A), decreased to 2068.4 cps after 30 minutes of milling (B), decreased to 1839.8 cps after 60 minutes of milling (C), and reached 1800.2 cps after 90 minutes of milling.

Referring to the research Keppetipola et al. (2021) and Rusma et al. (2024), which discusses the diffraction pattern of raw materials in coconut and Kluwak shells, the diffraction patterns of raw materials in rubber seed shells are the same as the diffraction patterns of raw materials in coconut and Kluwak shells. Figure 3 shows that the rubber shell-activated carbon has an amorphous structure. The peak on the graph is the peak of Carbon (C), which has formed a crystal with a hexagonal structure at 2-theta of about 22 degrees. From Figure 3, the diffraction peaks tend to decrease with increasing milling time. This shows the effect of the milling time on the crystallinity of the resulting activated carbon. The degree of crystallinity expresses the percentage of the crystal content in a material. The percentage of crystallinity of a sample can be determined by processing the XRD output data using the Method of Segmented Area (Peak Deconvolution) (Jasim and Ali, 2023; Nisa et al., 2023). The area of the crystalline diffraction peak compared to the total area (crystalline area + amorphous area). The formula for the degree of crystallization is as in Equation (8) below:

$$\text{Degree of Crystallinity (\%)} = \frac{A_{crystalline}}{A_{total}} \times 100\% \qquad (8)$$

where: $A_{crystalline}$ = area above baseline in the peak range (22°–28°)

A_{total} = the total area under the curve from $2\theta \sim 10°–80°$ ($A_{crystalline} + A_{amorphous}$)

The XRD analysis results show that the degree of crystallinity of activated carbon from rubber seed shells decreased slightly from 18.17% to 17.35% as the milling time increased from 0 to 90 minutes, as shown in Table 4. This decrease is relatively small, indicating that the material structure was initially dominated by the amorphous phase. This is consistent with the general characteristics of biomass-based activated carbon, which is typically formed from microcrystalline carbon domains (turbo-stratified graphite) dispersed in an amorphous matrix due to high-temperature carbonisation without further graphitisation.

The milling process plays a role in enlarging lattice defects and destabilising crystalline domains, as indicated by the decrease in diffraction peak intensity and the lack of significant change in the Bragg angle position. However, the milling energy used in this study appears to be insufficient to cause a drastic transformation of the crystalline structure into an amorphous one. In addition, the very small size of the crystalline domains (<5 nm) from the outset may also contribute to the low sensitivity of the degree of crystallinity to this mechanical treatment.

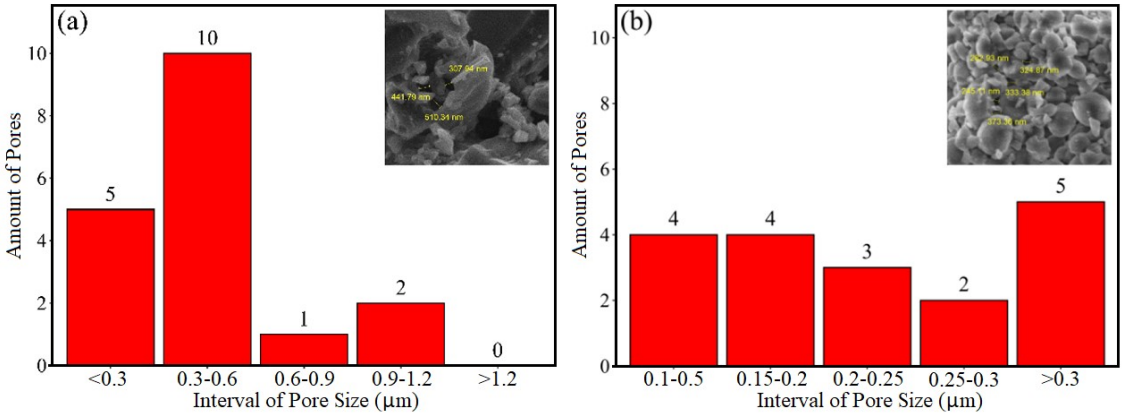

Figure 6. Bar Chart Showing Interval of Pore Size for (a) 30 Min of Milling and (b) 90 Min of Milling

Table 5. Comparison of Activation Methods, Post-Treatments, and Key Performance Parameters of Biomass-Derived Activated Carbon Reported in This Work and Selected Previous Studies

Study (year)	Raw material	Activation method & temperature	Milling / post-treatment	Advantages/notes
(Yang et al., 2020)	Oil palm shells	$ZnCl_2$ activation	No milling	Emphasizes micropores; this study emphasizes mesopore modification by HEM.
(Kengchuwong et al., 2023)	Rubber wood sawdust	KOH activation, 700°C	No milling	Strong chemical activation results in a high surface area; alternative to HEM.
(Jawad, 2018)	Rubber seed	One-step H_2SO_4 activation	Milling not reported	Practical, focused on application; focuses on pore modification via HEM.
(Aulia et al., 2019)	Rubber-seed shell	Carbonization 600°C	No HEM	Baseline study; this study added HEM for morphological control.
(Fatima et al., 2023)	Rubber-seed shell	Chemical activation	No Milling	Robust in modeling; this study shows physical effects of HEM.
(Nguyen et al., 2023)	Rubber-seed shell	Chemical + loading α-FeOOH	NO HEM	Specific composite; this study is a physical alternative to HEM without filler.
(Gao et al., 2024)	–	–	Discussion on milling parameters	This study applies the milling principle to specific biomass.
This study	Rubber-seed shell	Chemical; opt. 400–600°C	HEM 0–90 minutes	Combination of chemical activation + HEM; short milling reduces pore size

This finding is in line with the report by Suryanarayana (2001), in his book Mechanical Alloying and Milling, which states that a fully amorphous phase will form at high milling energies. Similarly, Gao et al. (2024) state that significant changes in crystallinity only occur if the initial structure has large graphitic domains or if milling is accompanied by thermal or catalytic activation. Therefore, in the context of activated carbon materials from rubber seed shells, the milling process functions more as an agent for increasing porosity and introducing microstructural defects than as a significant modifier of crystallinity.

To observe its surface morphology, rubber seed activated carbon was then examined using SEM. Figure 4 is an SEM image of activated carbon before milling with SEM image magnification of 1.14 kx (a) and 30 kx (b).

The morphology of activated carbon derived from rubber seed shells carbonised at 600 °C was examined using SEM at magnifications of 1.14 kx and 32 kx. From image (a) at low magnification (1.14 kx), the surface shows an irregular morphology with agglomerates, cracks, and voids formed during devolatilisation. These features indicate the initial development of pores in the early stages of carbonisation, although their dis-

tribution is not homogeneous. The presence of dense surface areas indicates that some pores are still clogged by tar residues or incomplete decomposition products, which is characteristic of biomass-based carbon carbonised at medium temperatures (Hassan et al., 2021).

The pores are more clearly visible and vary in size, ranging from micropores to mesopores, when the SEM magnification is increased to approximately 30 kx. The layered and irregular morphology is characteristic of the amorphous carbon structure obtained from lignocellulosic precursors after carbonisation (Vinod et al., 2023). However, some dense areas still exist, confirming that the pore network has not fully developed. This is consistent with previous reports that carbonisation at 600 °C generally produces initial porosity that requires further activation to increase surface area and pore accessibility (Hassan et al., 2021).

Therefore, although the SEM image confirms the formation of an initial porous structure consisting of micropores and mesopores at 600 °C, the material still requires further activation to optimise its adsorption performance. This trend has been widely reported in activated carbon derived from biomass, where the activation process transforms the initial porosity into a well-developed network suitable for the adsorption of heavy metals, organic contaminants, or CO_2 capture (Hassan et al., 2021; Vinod et al., 2023).

Figure 5 shows SEM images of rubber seed shell activated carbon, (a) before grinding, (b) grinding for 30 minutes, and (c) grinding for 90 minutes, each at 30× magnification. From Figure 5, the grinding time affects the particle size of the activated carbon. Before grinding, activated carbon from rubber seed shells had a single porous structure, surrounded by an uneven imprinted structure with a crater diameter of approximately 1.3 μm. The prominent pores in the centre may be a canal structure attached to the rubber seed shell (Shoba and Jeyanthi, 2022). The surface of the activated carbon shows large agglomerates with uneven porosity. These pores are partially clogged by tar residues from carbonisation, limiting surface accessibility. These observations are consistent with previous studies reporting that biomass-derived carbon carbonised at moderate temperatures (~500–700 °C) typically exhibits irregular morphology with underdeveloped pore networks (Hassan et al., 2021; Vinod et al., 2023).

After 30 minutes of grinding, the agglomerated structure began to break down into smaller particles, forming intraparticle pores with an average pore diameter of around 0.45 μm, thereby increasing the accessible surface area. However, some secondary agglomeration was still observed, possibly due to van der Waals interactions between fine particles. A similar trend of particle size reduction and pore opening during short-term mechanical grinding has been reported for materials derived from carbon and biomass (Gao et al., 2024).

After 90 minutes of grinding, the particles became more homogeneous and finer. The size of the intraparticle pores decreased significantly, with an average diameter of approximately 0.2 μm. SEM images showed more open and interconnected pores, indicating an increase in surface area and adsorption performance potential. However, prolonged grinding also caused partial re-agglomeration (cold welding) due to excessive impact energy, a phenomenon often observed in prolonged mechanical grinding of carbon powders (Gao et al., 2024). Overall, the SEM results indicate that grinding not only reduces particle size but also increases pore exposure, thereby enhancing the accessibility of adsorption sites.

Utilizing a thresholding-based image segmentation method by ImageJ to measure particle size, Figure 6 shows the distribution of activated carbon's intraparticle pore sizes after being milled for 30 and 90 minutes. The dispersion of pore sizes is centered below 0.6 μm in the 30-minute milling process; however, the pore sizes are more evenly dispersed in the 90-minute milling process. Large-sized chunk particles are still present, above 2 μm in size, as shown in Figure 5a, possibly due to uneven energy transfer from the milling balls to the material (Joy et al., 2022). In contrast, Figure 5b showed a homogeneous morphological structure of intraparticle pores; thus, it is decided that 90 minutes of milling is the optimal time for activated carbon material from rubber seed shell waste (Gohr et al., 2022).

This study makes an important contribution to processing rubber seed shell waste into activated carbon that can be used in various applications, such as adsorbents and filters. Variations in activation temperature show that activated carbon with maximum carbon content can be obtained at a temperature of 600 °C. This provides important information for optimising the production of activated carbon from rubber seed shell waste.

The main advantage of this research is the use of the high-energy milling (HEM) method, which has been proven effective in breaking down agglomerated structures into smaller particles and forming intraparticle pores. Increasing the milling time from 30 minutes to 90 minutes reduced the average pore diameter from approximately 0.45 μm to 0.2 μm with a more homogeneous intraparticle pore morphology. The HEM method shows great potential for industrial-scale production of cheaper and more environmentally friendly activated carbon by utilising abundant organic waste.

Table 5 presents a comparison between the present study and several previous works employing similar or different biomass precursors. Most earlier studies mainly focused on conventional chemical activation with various activating agents (e.g., KOH, H_2SO_4, $ZnCl_2$) or composite-based approaches (e.g., α-FeOOH), which successfully enhanced surface area or adsorption performance toward specific pollutants. However, none of these studies reported the application of mechanical post-treatment such as High-Energy Milling (HEM). In contrast, this work combines chemical activation of rubber seed shell at an optimum temperature of 600 °C with short-duration HEM treatment (30-90 minutes). The results demonstrate a reduction in average pore diameter from 0.45 μm to 0.20 μm, accompanied by a slight decrease in crystallinity (from 18.17% to 17.35%). This modification effectively refines the morphol-

ogy and is expected to enhance the accessible surface area without the need for additional chemical agents. Such an approach highlights the novelty and advantage of this study: offering a simple, energy-efficient, and effective physical route to improve the performance of biomass-derived activated carbon, which differs fundamentally from the chemical or composite-based strategies reported in earlier works.

4. CONCLUSIONS

The milling process using the HEM method causes cavitation in the activated carbon powder from rubber shells. From the XRD pattern, it can be seen that the diffraction peaks tend to decrease with increasing milling time. The diffraction intensity decreases when activated carbon is milled for 30 to 90 minutes. The diffraction intensity decreases because the crystal area of the activated carbon also decreases, which means that the crystal size decreases. From the crystallinity degree calculation results, the crystallinity of the rubber seed shell activated carbon decreases from 18.17% before milling to 17.35% after milling for 90 minutes. The SEM image also shows a decrease in the average pore diameter from approximately 0.45 μm to 0.20 μm with a more homogeneous intraparticle pore morphology structure when the milling time was increased from 30 minutes to 90 minutes.

5. ACKNOWLEDGEMENT

This research was conducted independently and fully supported by the authors' personal funds. The authors sincerely thank the reviewers for their constructive comments that helped improve the quality of this manuscript.

REFERENCES

Aulia, A., F. S. Arsyad, and A. Johan (2019). Temperature Carbonization Effect on the Quality of Activated Carbon Based on Rubber Seed Shell. In *Journal of Physics: Conference Series*, volume 1282. page 012043

Center for Agricultural Data and Information Systems (2020). Final December 2020 Rubber Outlook

Devi, R., V. Kumar, S. Kumar, M. Bulla, A. Jatrana, R. Rani, A. K. Mishra, and P. Singh (2023). Recent Advancement in Biomass-Derived Activated Carbon for Wastewater Treatment, Energy Storage, and Gas Purification: A Review. *Journal of Materials Science*, **58**(27); 12119–12142

Divya, M. P., S. Krishnamoorthi, R. Ravi, V. G. Jenner, K. Baranidharan, M. Raveendran, and P. Hemalatha (2025). Preparation and Characterization of Activated Carbon from Commercially Important Bamboo Species in North Eastern India. *Advances in Bamboo Science*, **11**; 100148

Fatima, S. S., A. Borhan, M. Ayoub, and N. A. Ghani (2023). Modeling of CO_2 Adsorption on Surface-Functionalized Rubber-Seed Shell Activated Carbon: Isotherm and Kinetic Analysis. *Processes*, **11**(10); 2833

Gao, P., X. Fan, D. Sun, G. Zeng, Q. Wang, and Q. Wang (2024). Recent Advances in Ball-Milled Materials and Their Applications for Adsorptive Removal of Aqueous Pollutants. *Water*, **16**(12); 1639

Gohr, M. S., A. I. Abd-Elhamid, A. A. El-Shanshory, and H. M. A. Soliman (2022). Adsorption of Cationic Dyes onto Chemically Modified Activated Carbon: Kinetics and Thermodynamic Study. *Journal of Molecular Liquids*, **346**; 118227

Hamid, M., T. I. Nasution, R. Elfinita, H. Wijoyo, and I. Isnaen (2024). Reducing Ammonia (NH_3) Levels in Fish Cage Water Using Activated Carbon Adsorbent Derived from Purple Corn Cob. *Science and Technology Indonesia*, **9**(3); 743–751

Hassan, U. F., A. A. Sallau, E. O. Ekanem, A. Jauro, and A. M. Kolo (2021). Effect of Carbonization Temperature on Properties of Char from Coconut Shell. *International Journal of Advanced Chemistry*, **9**(1); 34–39

Heimesaat, M. M., N. Schabbel, L. Q. Langfeld, N. W. Shayya, S. Mousavi, and S. Bereswill (2024). Prophylactic Oral Application of Activated Charcoal Mitigates Acute Campylobacteriosis in Human Gut Microbiota-Associated IL$-\frac{-/-}{10}$ Mice. *Biomolecules*, **14**(2); 141

Jasim, A. M. and N. A. Ali (2023). Microstructure Investigation of Activated Carbon Prepared from Potato Peel. *Journal of Applied Sciences and Nanotechnology*, **3**(2); 75–86

Jawad, A. H. (2018). Carbonization of Rubber (*Hevea brasiliensis*) Seed Shell by One-Step Liquid Phase Activation with H_2SO_4 for Methylene Blue Adsorption. *Desalination and Water Treatment*, **129**; 279–288

Joy, J., A. Krishnamoorthy, A. Tanna, V. Kamathe, R. Nagar, and S. Srinivasan (2022). Recent Developments on the Synthesis of Nanocomposite Materials via Ball Milling Approach for Energy Storage Applications. *Applied Sciences*, **12**(18); 9312

Kengchuwong, M., C. Ketwong, C. Nuasri, S. Wanich, S. Trisupakitti, and J. Morris (2023). Rubber Wood Sawdust Waste Converted to Activated Carbon for Heavy Metal Removal from Wastewater. *Journal of Food Health and Bioenvironmental Science*, **16**(1); 26–36. January–April 2023

Keppetipola, N. M., M. Dissanayake, P. Dissanayake, B. Karunarathne, M. A. Dourges, D. Talaga, L. Servant, C. Olivier, T. Toupance, S. Uchida, K. Tennakone, G. R. A. Kumara, and L. Cojocaru (2021). Graphite-Type Activated Carbon from Coconut Shell: A Natural Source for Eco-Friendly Non-Volatile Storage Devices. *RSC Advances*, **11**(5); 2854–2865

Li, L., X. Liu, K. Huang, Y. Wang, X. Zheng, J. Wang, Y. Du, L. Jiang, and S. Zhao (2020). A Facile Strategy to Fabricate Intumescent Fire-Retardant and Smoke Suppression Protective Coatings for Natural Rubber. *Polymer Testing*, **90**; 106689

Marcilla, A., S. García-García, M. Asensio, and J. A. Conesa (2000). Influence of Thermal Treatment Regime on the Density and Reactivity of Activated Carbons from Almond Shells. *Carbon*, **38**(3); 429–440

McEnaney, B. (1999). Structure and Bonding in Carbon Mate-

rials. In *Carbon Materials for Advanced Technologies*. Elsevier, pages 1–33

Milyutin, V. A., R. Bures, M. Faberova, and F. Kromka (2023). Effect of Milling Parameters on Size, Morphology, and Structure of Fe−Ga Binary Alloy Powder. *Journal of Materials Engineering and Performance*, **32**(9); 3839–3848

Mohan, V. L., S. M. S. Nagendra, and M. P. Maiya (2019). Photocatalytic Degradation of Gaseous Toluene Using Self-Assembled Air Filter Based on Chitosan/Activated Carbon/-TiO_2. *Journal of Environmental Chemical Engineering*, **7**(6); 103455

Neme, I., G. Gonfa, and C. Masi (2022). Activated Carbon from Biomass Precursors Using Phosphoric Acid: A Review. *Heliyon*, **8**(12); e11940

Nguyen, M. L., T. T. N. Hoang, D. T. Le, H. L. Ngo, N. T. T. Chau, and T. T. Nguyen (2023). Adsorption of Tetracycline Using the a-FeOOH-Loaded Rubber-Seed-Shell-Derived Activated Carbon. *Water, Air, & Soil Pollution*, **234**(9); 591

Nisa, Z. U., L. K. Chuan, B. H. Guan, F. Ahmad, and S. Ayub (2023). A Comparative Study on the Crystalline and Surface Properties of Carbonized Mesoporous Coconut Shell Chars. *Sustainability*, **15**(8); 6464

Nurfarhana, M. M., N. Asikin-Mijan, and S. F. M. Yusoff (2023). Porous Carbon from Natural Rubber for CO_2 Adsorption. *Materials Chemistry and Physics*, **308**; 128196

Oladipo, B. and E. Betiku (2020). Optimization and Kinetic Studies on the Conversion of Rubber Seed (*Hevea brasiliensis*) Oil to Methyl Esters over a Green Biowaste Catalyst. *Journal of Environmental Management*, **268**; 110705

Patel, H., A. Mohanty, and M. Misra (2024). Sustainable Synthesis of Activated Porous Carbon from Lignin for Enhanced CO_2 Capture: A Comparative Study of Physicochemical Activation Routes. *Energy Advances*, **3**(10); 2552–2568

Phiri, M. M., M. J. Phiri, K. Formela, and S. P. Hlangothi (2021). Chemical Surface Etching Methods for Ground Tire Rubber as a Sustainable Approach for Environmentally-Friendly Composites Development – A Review. *Composites Part B: Engineering*, **204**; 108429

Prasad, V. B. S. R., G. Venkatarao, and M. Idrees (2020). Identification of Damping Characteristics of EPDM-Rubber with Applications to Sandwiched Beams and Considerations to Engine Mounts for Performance Evaluation. *Materials Today: Proceedings*, **24**; 628–640

Roy, D., B. Roy, and A. K. Manna (2023). Pyrolyzed Mesoporous Activated Carbon Preparation from Natural Rubber Common Effluent Biosludge: Characterization, Isotherms, Kinetics, Thermodynamics, and ANN Modeling During Phenol Adsorption. *Groundwater for Sustainable Development*, **23**; 101020

Rusma, Y. S., P. Taba, S. Fauziah, M. Zakir, F. Samawi, and A. H. Assegaf (2024). Study into the Effectiveness of Using Activated Carbon of Kluwak Shell (*Pangium edule Reinw*) as Adsorbent of Heavy Metals in Wastewater. *Ecological Engineering & Environmental Technology*, **25**(9); 99–108

Sambasivam, K. M., P. Kuppan, L. S. Laila, V. Shashirekha, K. Tamilarasan, and S. Abinandan (2023). Kernel-Based Biodiesel Production from Non-Edible Oil Seeds: Techniques, Optimization, and Environmental Implications. *Energies*, **16**(22); 7589

Sarif, M., H. Bojet, T. Khadiran, R. Jalil, P. Elham, N. A. Lissem, J. Zainudin, W. C. Ching, and R. A. Dayus (2023). The Influence of H_3PO_4 Concentration on the Yield, Porous Structure, and Surface Chemicals of Sarawak Wild Bamboo Activated Carbon. *Malaysian Journal of Analytical Sciences*, **27**(5); 980–992

Sasmita, A., Edward, and D. Situmeang (2022). CO Adsorption Performance of Rubber Wood Activated Carbon. *Materials Today: Proceedings*, **63**; S26–S31

Shoba, B. and J. Jeyanthi (2022). Performance Analysis of Rubber Seed Shell Activated Carbon Incorporated Polymeric Membrane for the Separation of Oil-in-Water Emulsion. *Journal of Polymers and the Environment*, **30**(3); 1055–1071

Suryanarayana, C. (2001). Mechanical Alloying and Milling. *Progress in Materials Science*, **46**(1-2); 1–184

Swiątkowski, A., E. Kuśmierek, K. Kuśmierek, and S. Błazewicz (2024). The Influence of Thermal Treatment of Activated Carbon on Its Electrochemical, Corrosion, and Adsorption Characteristics. *Molecules*, **29**(18); 4930

Tarigan, J. B., R. Anggraini, R. P. Sembiring, M. Supeno, K. Tarigan, J. Ginting, J. A. Karo-karo, and E. K. Sitepu (2022). Waste Rubber Seeds as a Renewable Energy Source: Direct Biodiesel Production Using a Controlled Crushing Device. *RSC Advances*, **12**(4); 2094–2101

Togibasa, O., M. Mumfaijah, Y. K. Allo, K. Dahlan, and Y. O. Ansanay (2021). The Effect of Chemical Activating Agent on the Properties of Activated Carbon from Sago Waste. *Applied Sciences*, **11**(24); 11640

Tonu, N. T., S. Kundu, M. M. Islam, P. K. Dhar, T. Khandaker, M. A. A. M. Anik, S. K. Dutta, M. K. Hasan, and M. S. Hossain (2024). Fabrication of Waste Biomass-Derived KOH Activated Carbon for Enhanced CO_2 Capture. *New Journal of Chemistry*, **48**(43); 20212–20224

Torvorapanit, P., K. Kawang, P. Chariyavilaskul, S. J. Kerr, T. Chatsuwan, and V. Nilaratanakul (2023). The In Vitro Efficacy of Activated Charcoal in Fecal Ceftriaxone Adsorption among Patients Who Received Intravenous Ceftriaxone. *Antibiotics*, **12**(1); 127

Udo, M. D., U. Ekpo, and F. O. Ahamefule (2018). Effects of Processing on the Nutrient Composition of Rubber Seed Meal. *Journal of the Saudi Society of Agricultural Sciences*, **17**(3); 297–301

Vinod, A., H. Pulikkalparambil, P. Jagadeesh, and S. M. Rangappa (2023). Recent Advancements in Lignocellulose Biomass-Based Carbon Fiber: Synthesis, Properties, and Applications. *Heliyon*, **9**(3); e13614

Wardani, G. A., E. M. Qudsi, A. T. K. Pratita, K. Idacahyati, and E. Nofiyanti (2021). Utilization of Activated Charcoal from Sawdust as an Antibiotic Adsorbent of Tetracycline Hydrochloride. *Science and Technology Indonesia*, **6**(3); 214–221

Yang, Z., R. Gleisner, D. H. Mann, J. Xu, J. Jiang, and J. Y. Zhu (2020). Lignin-Based Activated Carbon Using H_3PO_4 Activation. *Polymers*, **12**(12); 2829

Yossaa, L. M. N., S. K. Ouimingaa, S. S. Sidibea, and I. W. K. Ouedraogo (2020). Synthesis of a Cleaner Potassium Hydroxide-Activated Carbon from Baobab Seeds Hulls and Investigation of Adsorption Mechanisms for Diuron. *Scientific African*, **9**; e00476

Zeng, B., X. Zeng, L. Hu, L. Huang, Y. Huang, Y. Zhou, G. Liu, and W. Huang (2024). Activated Carbon from *Camellia oleifera* Shells for Adsorption of Y(III): Experimental and DFT Studies. *RSC Advances*, **14**(6); 4252–4263

Zhu, L., Q. Wang, H. Wang, F. Zhao, and D. Li (2022). One-Step Chemical Activation Facilitates Synthesis of Activated Carbons from *Acer truncatum* Seed Shells for Premium Capacitor Electrodes. *Industrial Crops and Products*, **187**; 115458

Zuo, Q., Y. Zhang, H. Zheng, P. Zhang, H. Yang, J. Yu, T. J. Tang, Y. Zheng, and J. Mai (2019). A Facile Method to Modify Activated Carbon Fibers for Drinking Water Purification. *Chemical Engineering Journal*, **365**; 175–182

